Eur J Nucl Med Mol Imaging (2015) 42:1341–1352
DOI 10.1007/s00259-015-3075-9

ORIGINAL ARTICLE

Gene transcript analysis blood values correlate with ^{68}Ga-DOTA-somatostatin analog (SSA) PET/CT imaging in neuroendocrine tumors and can define disease status

L. Bodei[1] · M. Kidd[2] · I. M. Modlin[2] · V. Prasad[3] · S. Severi[4] · V. Ambrosini[5] · D. J. Kwekkeboom[6] · E. P. Krenning[6] · R. P. Baum[7] · G. Paganelli[4] · I. Drozdov[2]

Received: 27 January 2015 / Accepted: 21 April 2015 / Published online: 7 May 2015

Abstract
Purpose Precise determination of neuroendocrine tumor (NET) disease status and response to therapy remains a rate-limiting concern for disease management. This reflects limitations in biomarker specificity and resolution capacity of imaging. In order to evaluate biomarker precision and identify if combinatorial blood molecular markers and imaging could provide added diagnostic value, we assessed the concordance between ^{68}Ga-somatostatin analog (SSA) positron emission tomography (PET), circulating NET gene transcripts (NETest), chromogranin A (CgA), and Ki-67 in NETs.

Methods We utilized two independent patient groups with positive ^{68}Ga-SSA PET: data set 1 (^{68}Ga-SSA PETs undertaken for peptide receptor radionuclide therapy (PRRT), as primary or salvage treatment, n=27) and data set 2 (^{68}Ga-SSA PETs performed in patients referred for initial disease staging or restaging after various therapies, n=22). We examined the maximum standardized uptake value (SUV_{max}), circulating gene transcripts, CgA levels, and baseline Ki-67. Regression analyses, generalized linear modeling, and receiver-operating characteristic (ROC) analyses were undertaken to determine the strength of the relationships.
Results SUV_{max} measured in two centers were mathematically evaluated (regression modeling) and determined to be comparable. Of 49 patients, 47 (96 %) exhibited a positive NETest. Twenty-six (54 %) had elevated CgA (χ^2=20.1, $p<2.5\times10^{-6}$). The majority (78 %) had Ki-67<20 %. Gene transcript scores were predictive of imaging with >95 % concordance and significantly correlated with SUV_{max} (R^2=0.31, root-mean-square error=9.4). The genes *MORF4L2* and somatostatin receptors *SSTR1*, *3*, and *5* exhibited the highest correlation with SUV_{max}. Progressive disease was identified by elevated levels of a quotient of *MORF4L2* expression and SUV_{max} [ROC-derived AUC (R^2=0.7, $p<0.05$)]. No statistical relationship was identified between CgA and Ki-67 and no relationship with imaging parameters was evident.
Conclusion ^{68}Ga-SSA PET imaging parameters (SUV_{max}) correlated with a circulating NET transcript signature. Disease status could be predicted by an elevated quotient of gene expression (*MORF4L2*) and SUV_{max}. These observations provide the basis for further exploration of strategies that combine imaging parameters and disease-specific molecular data for the improvement of NET management.

Keywords ^{68}Ga-SSA PET · Chromogranin A · Gene transcripts · *MORF4L2* · NETest · Neuroendocrine

L. Bodei and M. Kidd contributed equally to this work.

Electronic supplementary material The online version of this article (doi:10.1007/s00259-015-3075-9) contains supplementary material, which is available to authorized users.

✉ M. Kidd
mark@wrenlaboratories.com

[1] Division of Nuclear Medicine, European Institute of Oncology, Milan, Italy

[2] Wren Laboratories, 35 NE Industrial Road, Branford, CT, USA

[3] Department of Nuclear Medicine, Charité University Hospital, Berlin, Germany

[4] Nuclear Medicine and Radiometabolic Units, Istituto Scientifico Romagnolo per lo Studio e la Cura dei Tumori (IRST) IRCCS, Meldola, Italy

[5] Nuclear Medicine, S.Orsola-Malpighi University Hospital, Bologna, Italy

[6] Nuclear Medicine Department, Erasmus Medical Center Rotterdam, Rotterdam, Netherlands

[7] THERANOSTICS Center for Molecular Radiotherapy and Imaging, Zentralklinik Bad Berka, Bad Berka, Germany

Introduction

Neuroendocrine tumors (NETs) have a relatively low incidence but an increasing frequency and prevalence. Their often indolent clinical course coupled with delayed detection can culminate in a late diagnosis, with metastatic progression [1, 2]. Limitations in imaging resolution as well as in the sensitivity and specificity of current blood and tissue biomarkers accentuate the clinical problem [3]. As a consequence, treatment outcomes have remained disappointing [4, 5]. Response to therapy is principally based on radiological criteria, which are challenging in "indolent" lesions since early measurable changes in tumor size are rare [6–8]. Alternative criteria, like attenuation measurements on CT (Choi criteria) initially proposed for gastrointestinal stromal tumors (GISTs), have been evaluated in NETs [9] but remain to be validated. Combinations of morphological and functional techniques, with ^{68}Ga-somatostatin analog (SSA) positron emission tomography (PET)/CT, are also under consideration [10, 11].

Circulating biomarkers, e.g., chromogranin A (CgA), are currently used despite the lack of reproducibility and high variability [3, 12]. The prognostic value of histopathological parameters, e.g., Ki-67 index, has been validated in a number of studies and is generally accepted as the best currently available histopathological parameter for assessment of tumor grading [13]. However, the intratumoral heterogeneity in proliferative rates and the clinical difficulties related to repeated assessments remain as limiting factors for Ki-67 [14]. An alternative to the measurement of single analytes is the novel strategy of multianalyte assays with algorithmic analyses (MAAA) [15]. In this respect, a polymerase chain reaction (PCR)-based blood biomarker test that captures the expression levels of the spectrum of transcripts has been described [16]. This assay defines the circulating "fingerprint" of a NET [17] and exhibits a high sensitivity and specificity (98 and 97 %, respectively) for identifying NETs. The assay is standardized and highly reproducible (inter- and intra-assay coefficient of variation <2 %) and is independent of tumor heterogeneity [18].

An amalgamation of biomarker and imaging technologies may provide an opportunity to optimize accurate detection and early determination of disease progress [19, 4]. We hypothesized that imaging and biomarkers may capture similar biological information and that combinations of this information could be of clinical utility. We therefore evaluated the concordance of two of the most sensitive and specific methods of NET diagnosis, ^{68}Ga-SSA PET/CT and the blood-based PCR assay (NETest) in NET disease and assessed whether they correlated with tissue and blood biomarkers. Our aims were to: (1) evaluate whether the circulating gene transcripts correlated with imaging parameters (the maximum standardized uptake value, SUV_{max}), (2) identify the relationship between gene expression levels or SUV_{max} and circulating CgA, and (3) examine if the NETest was a surrogate marker for tumor proliferation (Ki-67). Additionally, we determined whether a combination of imaging and the NETest provided an index that had clinical utility for the assessment of disease progression.

Materials and methods

Patients

Two independent groups of metastatic NETs that demonstrated measurable disease by ^{68}Ga-SSA PET/CT were studied. Data set 1 (n=27) included patients who were referred before (0–30 months, median 3) peptide receptor radionuclide therapy (PRRT), which was performed as primary or salvage treatment (IEO Milan, IRST Meldola; Table 1A). Data set 2 (n=22) included patients who were referred for initial disease staging or for restaging after various therapies (Charité University, Berlin; Table 1B). Information in Table 1 included Ki-67, the tissue and method utilized for Ki-67 assessment (surgery, biopsy, or cytology), grading, tumor functionality, disease duration, and performance status according to the Eastern Cooperative Oncology Group (ECOG) [20]. All patients provided informed consent for the translational analysis, which was authorized by the local Ethics Committees [Authorization IRST-70/12 (data set 1) and EA2_064_09 (data set 2)]. Status at baseline was assessed according to RECIST1.1 criteria [21]. The demographics and disease characteristics of the entire group are included in Table 2.

Somatostatin receptor (SSTR) imaging

^{68}Ga was eluted from ^{68}Ge/^{68}Ga generators and labeled with DOTATATE, DOTATOC, or DOTANOC. ^{68}Ga-SSA PET/CT was performed following the European Association of Nuclear Medicine (EANM) Guidelines [22].

Image acquisition

For Data set 1 (^{68}Ga-DOTATOC), a GE Discovery 600 (#1), Discovery ST (#2), Discovery LS (#3), or Discovery STE (#4) PET/CT scanner was used (GE Healthcare, Milwaukee, WI, USA). The acquisition protocol included a low-dose CT (120 kV, 80 mA, 0.8 s/rotation, 1.35 pitch, 3.75-mm slice thickness) for attenuation correction followed by the whole-body PET scan (5–6 beds/3 min each). Scanners #1, #2, and #4 acquired in 3-D mode (256×256 matrix, VUE point attenuation-weighted ordered subset expectation maximization (OSEM) algorithm, smoothing Gaussian filter), while scanner #3 acquired in 2-D mode (128×128 matrix, same reconstruction). For data set 2 (17 ^{68}Ga-DOTATATE, 4

Table 1 Patients' characteristics

Primary	Age (years)	Sex	Ki-67	Sample for Ki-67	Grading	Syndrome	Disease duration (months)	PS	Status at baseline	CgA	Previous therapies	Scanner	Peptide
Patients selected for PRRT (data set 1)													
Rectum	49	M	15 %	S, primary, liver, LN	G2	No	26	0	PD	13	Surgery, RFA, SSA	1	TOC
Unknown	43	F	n.a.	C, liver	G1/G2	Carcinoid	17	0	PD	16	TAE, SSA	2	TOC
Small intestine	49	F	n.a.	S, primary, LN	G1/G2	Carcinoid	107	0	PD	83	Surgery, TAE, Y-PRRT, SSA	2	TOC
Small intestine	57	M	12 %	B, peritoneum	G2	Carcinoid	14	1	PD	157	Bypass surgery, chemo, SSA	4	NOC
Small intestine	75	M	13 %	S, LN	G2	No	8	0	SD	20	Lu-PRRT	1	TOC
Pancreas	67	M	3 %	S, primary, LN	G2	No	3	0	SD	15	Surgery, SSA	4	NOC
Small intestine	65	M	<1 %	S, primary	G1	No	48	0	PD	93	Surgery	3	TOC
Bronchial	73	M	3 %	S, primary, liver	Atypical carcinoid	Carcinoid	110	1	PD	701	Surgery, chemo, SSA	3	TOC
Rectum	64	F	20 %	S, primary, liver	G3	Carcinoid	46	0	PD	11	Surgery, RFA, Lu-PRRT, SSA	2	TOC
Colon	53	F	5 %	B, liver	G2	No	47	0	PD	9	Surgery, chemo, Lu-PRRT, SSA	4	NOC
Small intestine	62	M	19 %	S, primary, LN, liver	G2	Carcinoid	64	0	PD	481	Surgery, chemo, Lu-PRRT, sunitinib, SSA	3	TOC
Small intestine	73	F	<1 %	S, primary, LN	G1	Carcinoid	174	1	PD	11	Surgery, chemo, Y-PRRT, SSA	3	TOC
Bronchial	74	M	n.a.	B, primary	High grade	No	6	0	PD	25	Chemo, EBRT	2	TOC
Pancreas	66	M	n.a.	S, primary, liver	G1/G2	No	22	0	PD	15	Surgery, Lu-PRRT, SSA	1	TOC
Bronchial	75	M	(MI: 4/10 HPF)	S, primary, LN	Atypical carcinoid	No	55	1	PD	615	Surgery, EBRT, Lu-PRRT	4	NOC
Pancreas	63	M	4 %	B, liver	G2	No	50	1	PD	11	Chemo, Lu-PRRT, SSA	1	TOC
Duodenum	73	M	2 %	B, primary	G1	No	132	1	PD	531	SSA, IFN	1	TOC
Small intestine	63	F	<1 %	S, liver	G1	Carcinoid	129	0	SD	385	Surgery, TACE, Y-PRRT, SSA	3	TOC
Pancreas	57	F	25 %	B, primary, liver	G3	No	1	0	n.a.	141	Chemo	3	TOC
Small intestine	73	M	15 %	B, liver	G2	Carcinoid	7	1	PD	712	SSA	3	TOC
Pancreas	71	M	n.a.	S, primary	G1/G2	No	212	0	PD	28	Surgery, Y-PRRT, Lu-PRRT, EBRT, everolimus	1	TOC
Bronchial	77	F	21 %	S, primary, LN, B, liver	Atypical carcinoid	No	41	0	SD	410	Surgery, chemo	1	TOC
Unknown	74	M	5 %	S, liver	G2	No	80	1	PD	496	Liver surgery, Lu-PRRT, SSA	3	TOC
Small intestine	75	M	1 %	B, liver	G1	Carcinoid	150	0	SD	377	Surgery, chemo, EBRT, SSA	3	TOC
Small intestine	74	M	15 %	B, liver	G2	Carcinoid	73	0	PD	962	Surgery, RFA, everolimus, SSA	4	NOC
Small intestine	55	M	12 %	B, primary, liver and peritoneum	G2	No	0	0	PD	643	SSA	1	TOC
Bronchial	66	M	<1 %	S, primary	Atypical carcinoid	No	80	0	PD	169	Surgery, SSA	3	TOC
Patients in staging or restaging (data set 2)													
Small intestine	57	F	1 %	S, primary	G1	Carcinoid	221	0	SD	11	Surgery, RFA, SSA	B	TOC

Table 1 (continued)

Primary	Age (years)	Sex	Ki-67	Sample for Ki-67	Grading	Syndrome	Disease duration (months)	PS	Status at baseline	CgA	Previous therapies	Scanner	Peptide
Small intestine	55	M	9 %	B, liver	G2	Carcinoid	6	0	SD	280	SSA	A	TATE
Pancreas	70	F	30 %	S, primary	G3	No	7	0	SD	35	Surgery, chemo	A	TATE
MEN1	47	F	1 %	S, primary	G1	ZES	51	0	SD	6947	Surgery	A	TATE
Small intestine	58	M	2 %	S, primary	G1	No	7	0	SD	45	Surgery	A	TATE
Pancreas	72	F	5 %	S, primary	G2	No	84	0	PD	47	Surgery	A	TATE
Pancreas	32	F	10 %	B, LN	G2	No	15	1	PD	62	SSA	A	TATE
Pancreas	53	F	5 %	B, liver	G2	No	0	0	PD	190	None	A	TATE
Pancreas	43	M	9 %	S, primary	G2	No	11	0	SD	43	Surgery	A	TATE
Pancreas	54	F	2 %	S, primary	G1	No	26	0	PD	48	None	A	TATE
Small intestine	64	M	2 %	S, liver	G1	No	18	0	SD	33	None	A	TATE
Cecum	55	F	5 %	S, primary	G2	Carcinoid	284	0	SD	68	Surgery, SSA	B	TATE
Small intestine	62	F	1 %	S, primary	G1	Carcinoid	84	0	PD	769	Surgery, SSA	B	TATE
Small intestine	62	M	5 %	S, primary	G2	Carcinoid	43	0	SD	156	Surgery, SSA, everolimus	B	TATE
Small intestine	66	F	10 %	S, liver	G2	Carcinoid	132	0	SD	55	Surgery, SSA	B	TATE
Small intestine	68	M	2 %	S, LN	G1	Carcinoid	54	0	SD	413	Surgery, vatalanib	B	TATE
Cecum	56	F	5 %	S, primary	G2	Carcinoid	289	1	PD	68	Surgery, SSA	B	TATE
Small intestine	57	F	1 %	S, liver	G1	No	5	0	PD	90	Surgery	B	TATE
Pancreas	73	F	30 %	S, primary	G3	No	39	1	PD	47	Chemo, surgery	B	TATE
Small intestine	66	F	2 %	S, primary	G1	Carcinoid	91	0	SD	16	Surgery, SSA	B	TOC
Small intestine	48	M	2 %	B, liver	G1	Carcinoid	47	0	SD	101	Surgery, SSA, Lu-PRRT	B	TOC
Small intestine	58	M	10 %	S, primary	G2	Carcinoid	221	0	SD	138	Surgery, SSA, Lu-PRRT	B	TOC

B biopsy, *LN* lymph node, *C* cytology, *S* surgery, *MI* mitotic index, *HPF* high-power field, *ZES* Zollinger-Ellison syndrome, *PS* performance status according to ECOG criteria [20], *PD* progressive disease, *SD* stable disease, *n.a.* not assessed, *chemo* chemotherapy, *EBRT* external beam radiotherapy, *IFN* interferon, *Lu- or Y-PRRT* peptide receptor radionuclide therapy with either ^{177}Lu or ^{90}Y, *RFA* radiofrequency ablation, *SSA* somatostatin analogs, *TAE* transcatheter arterial embolization, *MEN1* multiple endocrine neoplasia 1, *TA(C)E* transarterial (chemo)embolization, scanners *1* GE Discovery 600, *2* Discovery ST, *3* Discovery LS, *4* Discovery STE, *A* Siemens Biograph 16, *B* Philips Gemini TF-16, peptides, *TOC* ^{68}Ga-DOTATOC, *NOC* ^{68}Ga-DOTANOC, *TATE* ^{68}Ga-DOTATATE

Table 2 Baseline demographic and disease characteristics of the entire group

Patients	(*n*=49)
Age, years, median (range)	63 (32–77)
Men	27 (55 %)
Time since diagnosis, months (range)	0–289
Median	47
NET origin	
Small bowel	23 (47 %)
Pancreas	12 (24 %)
Colon	3 (6 %)
Rectum	2 (4 %)
Unknown	2 (4 %)
MEN1	1 (2 %)
Duodenum	1 (2 %)
Bronchopulmonary	5 (10 %)
Tumor grade (*n*=44)[a]	
G1	15 (34 %)
G2	21 (48 %)
G3	4 (9 %)
Not specified	4 (9 %)
Bronchopulmonary classification (*n*=5)[b]	
Typical	0 (0 %)
Atypical	4 (80 %)
High-grade	1 (20 %)
Clinical stage IV	49 (100 %)
Baseline RECIST status	
Progressive	29 (59 %)
Stable	19 (39 %)
n.a.	1 (2 %)
Previous therapies	
Primary tumor surgery	33 (67 %)
SSA	30 (61 %)
Other surgical treatments	
Liver surgery	1 (2 %)
Jejunoileal bypass	1 (2 %)
Prior nonsurgical treatment except SSA	
PRRT	13 (27 %)
Chemotherapy	12 (24 %)
Liver-directed therapies	6 (12 %)
Targeted therapies	4 (8 %)
Radiotherapy	3 (6 %)
IFN	1 (2 %)

MEN1 multiple endocrine neoplasia 1, *n.a.* not assessed, *IFN* interferon

[a] Grading according to WHO 2010 classification was assessed in the 44 GEP NETs [24]

[b] According to 2004 Travis classification [25]

^{68}Ga-DOTATOC) two different scanners were used. A Biograph 16 (Siemens AG, Erlangen, Germany; 120 kV, 230 mAs, 5–6 bed position/3 min, 0.75 mm collimation, and 0.75-mm slice thickness) was used in 2008–2009 (scanner A). Thereafter, (2010 to present) a 3-D Gemini TF-16 PET/CT (Philips Medical Systems, scanner B) was used. The 3-D line-of-response (LOR) algorithm of the system software was used to reconstruct the images (transaxial slices: 144×144 voxels, 4.0×4.0×4.0 mm^3). A pre-scan low-dose CT was used for attenuation correction (120 kVp, 30 mAs).

Quantitative image analyses

PET images were interpreted by two nuclear medicine physicians (VP, LB) with >10 years of experience. The SSR expression in tumor was assessed using a semiquantitative method (SUV_{max}). These were measured using a spherical region of interest (ROI) in a transaxial attenuation-corrected PET slice in those lesions that were positive on the visual assessment, i.e., uptake more than the immediate normal surrounding tissue. The uptake in the normal liver was used as a reference value for tumor SUV_{max} normalization [23]. To avoid the partial volume effect, only lesions >1.5 cm, based on the coregistered CT, were considered.

Multianalyte algorithm analysis (MAAA) PCR-based test (NETest)

A two-step protocol (RNA isolation, cDNA production, and PCR) was used as described [16]. Transcripts (mRNA) were isolated from 1 ml ethylenediaminetetraacetic acid (EDTA)-collected whole blood samples using the Blood Mini Kit (Qiagen, Valencia, CA, USA). Real-time PCR (50 °C 2 min, 95 °C 10 min, then 95 °C 15 s, 60 °C, 60s for 40 cycles) as described [16, 18] was performed (384-well plate, HT-7900 machine) with 200 ng/μl of cDNA and 16 μl of reagents/well (Fast Universal PCR Master Mix, Life Technologies, Carlsbad, CA, USA). All primers used were exon spanning and are <150 base pairs recognition sequence (bprs). PCR values were normalized to housekeeping genes and expression was quantified against a population control (calibrator sample). Four different learning algorithms trained on the internal training set using upregulated features were used and resulted in a consensus categorization of samples into different groups using "majority vote" methodology. A NET score (0–8) was derived from the PCR data using MATLAB (R2011a, MathWorks, Natick, MA, USA) [17]; a value ≥2 is a positive tumor score [17, 18].

CgA assay

CgA was measured using the DAKO CgA enzyme-linked immunosorbent assay (ELISA) kit (DAKO, Carpinteria, CA, USA). A cutoff of 19 units/l defined the upper limit of normal [16].

Ki-67 proliferation index

The Ki-67 value was obtained from the original histopathological reports. In some cases the classification of NETs was revised. The WHO 2010 classification was taken into account for gastroenteropancreatic (GEP) tumors while the 2004 Travis classification was used for bronchial forms [24, 25].

Statistical analyses

Comparative analysis of SUV_{max}, CgA, and Ki-67 across data sets 1 and 2 was undertaken using the Kolmogorov-Smirnov test of equality of continuous one-dimensional distributions to determine if values of each parameter were drawn from the same underlying distribution, regardless of the data set origin. A two-sample test (null hypothesis: x and y drawn from the same continuous distribution) was performed; *p* values approaching 1 signified statistically identical distributions. Numerical predictions of Ki-67 and SUV_{max} using gene expression profiles were produced by fitting a generalized linear model via penalized maximum likelihood ("glmnet" [26]) to the training data set (set 1), implemented in the "caret" R package [27]. Model tuning parameters were estimated in caret by minimizing root mean square error (RMSE). Variable importance was calculated using the caret "varImp" function specific to the glmnet package. Regression models were tested on data set 2. In the instances where *t* variables (e.g., Ki-67 and CgA) were identified as noncompatible (significantly different) between data sets 1 and 2, the regression model was trained on the combined data set (data set 1+data set 2) and model performance was estimated using five repeats of 10-tenfold cross-validation. Combinatorial assessments were undertaken using the SUV_{max} and *MORF4L2* expression, Ki-6,7 and CgA. Sensitivity comparisons were undertaken using χ^2, nonparametric measurements and receiver-operating characteristic (ROC)/AUC (continuous variables) analysis. Both Prism 6.0 for Windows (GraphPad Software, La Jolla, CA, USA, www.graphpad.com) and MedCalc Statistical Software version 12.7.7 (MedCalc Software, Ostend, Belgium, http://www.medcalc.org; 2013) were utilized. AUCs were compared and the Z-statistic derived (MedCalc) [28].

Results

Positive ^{68}Ga-SSA PET/CT scans were available in all patients. Of 49 patients, 47 (96 %) exhibited a positive NETest, while 26 (54 %) had elevated CgA levels (χ^2=20.1, $p<2.5\times10^{-6}$). The MAAA score was significantly associated with image positivity (>95 % concordance), while CgA levels were non-predictive.

Quality control and data processing

We initially examined whether the SUV_{max}, the circulating 51-gene expression profiles, plasma CgA levels, and tissue Ki-67 were statistically comparable between the two data sets. Principal component analysis of 51 marker gene expression profiles identified that one sample in data set 1 was an outlier. This sample, a bronchial tumor—small cell lung carcinoma (SCLC)—was removed (Fig. 1a). Results of the two-sample Kolmogorov-Smirnov test of equality indicated that SUV_{max} were comparable (p=0.546) between the two data sets (Fig. 1b), while neither CgA (p=0.165) nor Ki-67 values (p=0.0535) were mathematically comparable (Fig. 1c, d).

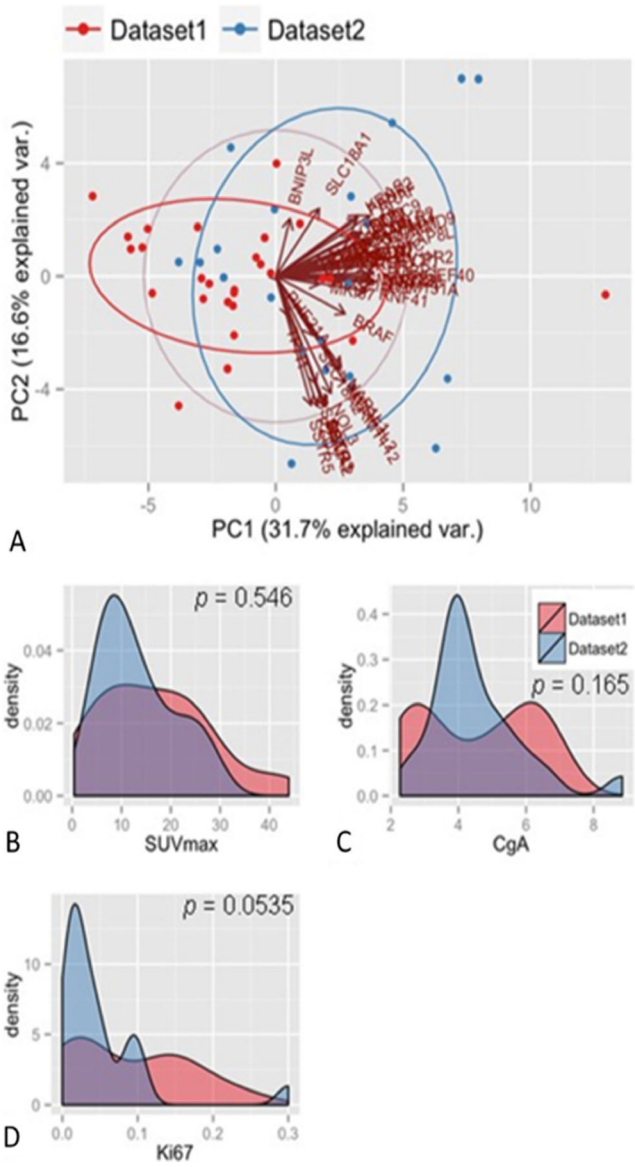

Fig. 1 Principal component analysis of data set 1 and data set 2 (**a**) using expression profiles of 51 marker genes. One outlier sample was excluded. Distribution densities of SUV (**b**), CgA (**c**), and Ki-67 (**d**) in data sets 1 and 2 confirmed the comparability of SUV_{max} but not of Ki-67 or CgA

Based on the mathematically defined acceptable comparability, we then merged the two data sets to mathematically amplify data analysis.

Chromogranin A

Although CgA levels were poorly reproducible (Kolmogorov-Smirnov p=0.165) between the two data sets, we examined if the marker genes could predict these values. For this analysis, the regression model was trained on data set 1 and validated on data set 2. Utilizing the mathematical model of "feature importance selection," *SLC18A2* and *LED1* were identified as circulating marker transcripts that could be used to predict CgA levels (Fig. 2a, b). The overall regression model was R^2=0.13 and RMSE=1.47 (Fig. 3a).

Histopathology and Ki-67

Regression analysis of Ki-67 values and circulating marker gene expression (combined data sets) failed to identify any significant relationships. In addition, Ki-67 levels could not be extrapolated by generalized linear regression modeling. A similar result was arrived at when data sets 1 and 2 were interrogated individually. No relationships could be identified between Ki-67 and CgA or between the SUV_{max} and Ki-67 using the same modeling approaches.

Somatostatin receptor imaging

We next examined whether circulating marker gene expression could be used to predict the SUV_{max}. Given the SUV_{max} were comparable between the two data sets (see Fig. 1), data set 1 was used to train the generalized linear regression model, while data set 2 was used as a test. In the training model, the transcript *MORF4L2* was the most effective predictor of the SUV_{max} (Fig. 2c, d). A regression of R^2=0.31 and RMSE=9.4 was identified (Fig. 3b). An assessment of the combined data set indicated that among expression levels of *SSTR1*, *3*, and *5*, the latter was the single most important predictor of SUV_{max} (R^2=0.15 and RMSE=9.5). Neither CgA levels nor Ki-67 were predictive of SUV_{max} (Fig. 4).

Combinatorial assessments

To examine whether circulating marker levels and imaging could be used in combination, we evaluated different combinations of gene expression levels and the SUV_{max} to predict disease status, e.g., stable disease according to RECIST1.1 criteria [21]. While neither a CgA-based nor Ki-67-weighted

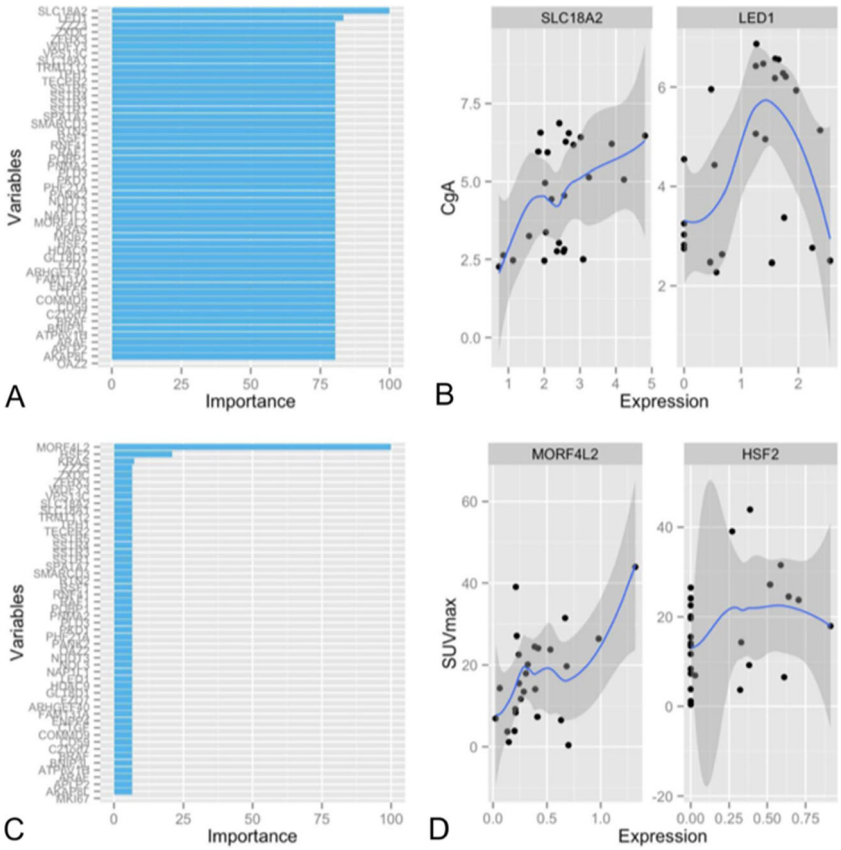

Fig. 2 Bar plots of top contributing genes to prediction of CgA and SUV_{max} levels (**a**, **c**). Scatter plots of expression levels of top contributing genes and CgA and SUV_{max} levels in data set 1 (**b**, **d**). *SLC18A2* and *LED1* were identified as key marker genes for CgA, while *MORF4L2* was the most effective predictor of SUV_{max}. Linear regression lines for each scatter plot are shown in *blue*, while 95 % confidence regions are shaded in *gray*

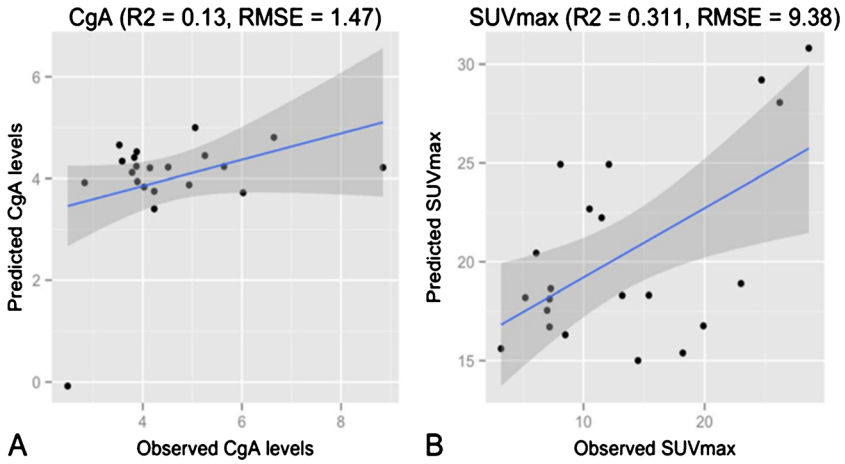

Fig. 3 Scatter plots of predicted and actual CgA and SUV_{max} values (**a**, **b**). A good regression was identified for both. Linear regression lines for each scatter plot are shown in *blue*, while the 95 % confidence regions are shaded in *gray*

score correlated with the clinical status, the *MORF4L2*-calculated quotient (a combination of circulating transcript expression and the SUV_{max}) was significantly elevated in progressive disease ($p<0.03$). This quotient also exhibited significant ROC-derived AUCs ($R^2=0.7$, $p<0.05$) when combined with SUV_{max} (Fig. 5, Table 3).

Discussion

We evaluated whether SSR-based imaging and blood or tissue biomarker measurements in NETs provided complementary information by assessing the degree of the correlation between each of these parameters. We also examined whether combinations of imaging and these biomarkers provided clinically useful information. Our results demonstrated that the SSR imaging parameter, SUV_{max}, and the NET marker gene panel were well correlated, capturing similar biological data. Moreover, a combination of circulating transcript levels, particularly *MORF4L2*, and imaging effectively differentiated progressive from stable disease. No statistical relationship could be identified between imaging parameters and either CgA or Ki-67 or between the NETest and these two measurements.

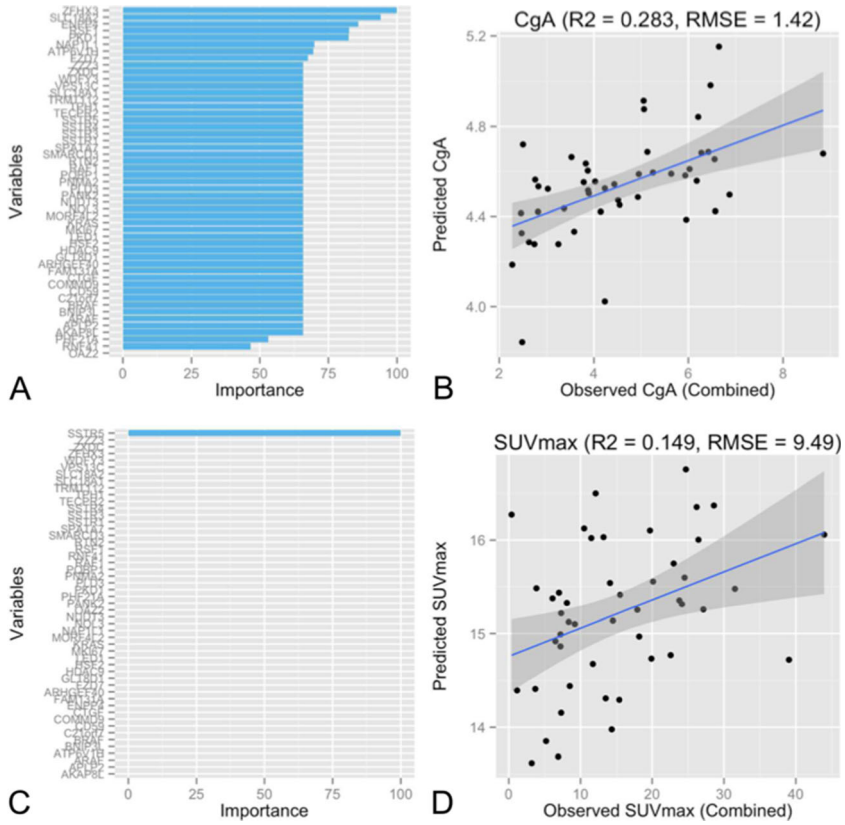

Fig. 4 Bar plot of top contributing genes to predicting of CgA and SUV_{max} levels in the combined data set (data sets 1 and 2) (**a**, **c**). Scatter plot of predicted and actual CgA and SUV_{max} values in the combined data set (**b**, **d**). Linear regression lines for each scatter plot are shown in *blue*, while the 95 % confidence regions are shaded in *gray*

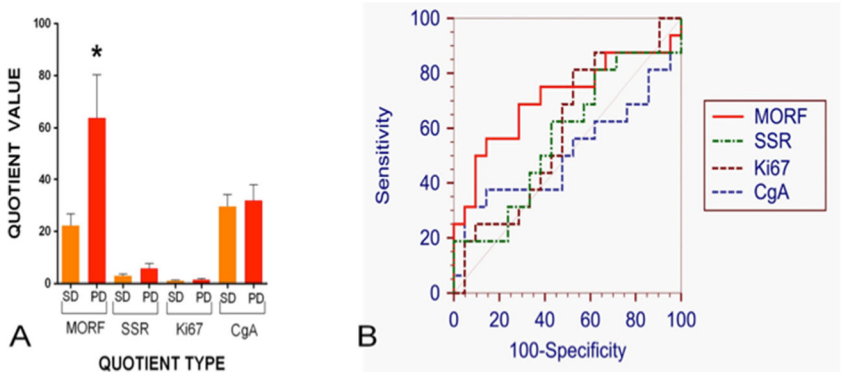

Fig. 5 Expression differences and ROC curves for the four different quotients. **a** The *MORF4L2* quotient value was significantly increased in progressive disease (n=24) patients compared to those with stable disease (n=25). **b**) The AUC for the SUV_{max} *MORF4L2* quotient was 0.71 compared to quotients assessing averaged SSR expression and either Ki-67 index or CgA. *p<0.05 vs stable disease. *MORF MORF4L2* quotient, *SSR* averaged SSR expression quotient, *Ki-67* Ki-67 indexed quotient, *CgA* chromogranin A-calculated quotient

This effort to examine the correlations between imaging parameters and circulating transcripts has a number of strengths and weaknesses. The principal strength is the demonstration that it is feasible to combine information from two separate sources, namely, SSR-based imaging and molecular information. Three-dimensional lesion localization and ^{68}Ga-SSA PET quantification of SSTR density can be related to the multidimensional data from the measurements of specific circulating tumor transcripts. Thus, two objectively quantifiable parameters obtained in two different compartments (blood and tumor tissue) exhibit a mathematically definable relationship directly related to the biological parameters of disease. The clinical implication is that it identifies the possibility of developing sensitive bidimensional diagnostic protocols for the management of NETs.

A weakness of the study is the use of a retrospective patient series and the limited number of cases available for evaluation and the lack of homogeneity of the histopathological assessment of some of the cases, which may have diminished the effectiveness of the evaluation of Ki-67. Nevertheless, the observations derived from this study support undertaking a larger prospective series. This should prospectively evaluate a combination of ^{68}Ga-SSA PET and NET transcripts tested against the long-term outcome. An important caveat would be to ensure comparability of SSR imaging. In this series, it was evident that imaging parameters obtained from ^{68}Ga-DOTANOC were not optimally mathematically comparable with ^{68}Ga-DOTATOC and ^{68}Ga-DOTATATE (Supplemental Fig. 1). Although this may represent the different receptor binding affinities of the individual peptides, it may also reflect the limited number of patients available for evaluation and would require a more detailed, prospective assessment.

Table 3 Performance metrics for the combinatorial quotients

	AUC	SE[a]	95 % CI[b]
MORF4L2	0.708	0.0926	0.536–0.846
SSR	0.568	0.0978	0.396–0.730
Ki-67	0.589	0.0956	0.416–0.748
CgA	0.512	0.104	0.396–0.730

CI confidence interval

[a] Hanley and McNeil [28]

[b] Exact binomial

^{68}Ga-SSA PET is used for localization, staging, and selection for SSR-based therapies. The pooled sensitivity and specificity is >90 % [29]. The resolution sensitivity (~5-6 mm) and a threshold for partial volume effect ≥1 cm with the newer PET/CT systems, however, limit the ability to detect small changes in tumors [30, 22]. This is a concern when seeking to identify a therapeutic response in an often indolent disease process. A prognostic use for ^{68}Ga-SSA PET/CT, particularly measurements of the SUV_{max}, has been suggested for predicting responses to SSA or PRRT [31, 32] or for predicting progression-free survival (PFS). These data need to be both standardized, i.e., similar measurements at different institutions, and would require prospective confirmation in larger series [33]. Similar information has also been obtained from use of the OctreoScan, where the uptake classified according to the "Krenning scale" generally correlates with the response to PRRT. In this case, a grade 4 uptake is predictive of response to PRRT in 60 % of individuals [34]. An improvement in these measures is clearly required. Imaging also provides prognostic data because it identifies SSTR expression. The latter, however, does not directly reflect the proliferation characteristics of the tumor cells. This is based upon the individual unique proliferome of a tumor, which is a complex multiplex of genomic regulators [35], and is important for predicting therapeutic responsiveness, e.g., low proliferative tumor does not respond to chemotherapeutics [1].

The SUV is a widely accepted metric for assessing tissue accumulation of tracers. In the current study, we considered the SUV_{max} per body weight since there is no differential

biodistribution of SSA based on lean body mass or body surface. We identified that the SUV_{max} could be predicted by measurements of circulating gene markers (R^2>0.3, RSME=9.4). The detection of specific NET transcripts in circulating blood therefore correlates with the level of uptake at ^{68}Ga-SSA PET. Rather than implying the possibility of substituting either technique with the other (the overlap in biological data captured is ~30 %), this observation rather suggests an "information complementarity." Developing the appropriate tools to define this prospectively could be used to both facilitate diagnostic assessment as well as improve patient selection for therapy of SSR-expressing tumors.

The ^{68}Ga-DOTATOC SUV_{max} is biologically related to expression of transcript and protein for *SSTR2* in tumors, and a close correlation has been noted between SUV_{max} and immunohistochemical SSTR scores in NET tissue (p<0.001 and p<0.05 for *SSTR2A* and *SSTR5*, respectively) [36]. The NETest gene panel does not include measurements of circulating expression of *SSTR2*. This gene is ubiquitously expressed in normal blood cell populations, e.g., leukocytes [37], and circulating levels from tumor cells cannot be consistently differentiated because of the preexisting expression in whole blood (Kidd, Modlin: unpublished data). Expressions, however, of *SSTR1*, *3*, and *5* are transcript components of the NETest and contribute to the regression model that predicts the SUV_{max} (Fig. 2a). In this respect it appears that the *SSTR5* subtype is of significance. Irrespective of the SSR subtype target, ^{68}Ga-DOTATOC and ^{68}Ga-DOTATATE have been reported to exhibit a comparable diagnostic accuracy for NET detection [38]. These observations are consistent with our identification that expression of clinically relevant SSR genes, particularly *SSTR5*, is biologically informative regarding the receptor density of the tumor in situ.

We noted that expression levels of *MORF4L2* were an important component of the predictive model for the $SUV_{max.}$ This gene is involved in telomere homeostasis via the regulation of cellular transcription through chromatin remodeling [39]. Since telomere "health" has been related in pancreatic NETs to tumor differentiation and therefore prognosis [40], there exists sound biological rationale for considering that *MORF4L2* expression may be related to SSR density and radiolabeled peptide uptake. Higher uptake of SSR peptides has been demonstrated as predictive of well-differentiated NET response to SSR-based therapy [41, 31]. In this study, assessments of a candidate quotient—expression of *MORF4L2* and SUV_{max}—demonstrated potential utility as a measure of disease progression, independent of the comparison with the previous or subsequent exam. A possibility worth examining is that a combination of clinical imaging methods with validated molecular biomarkers could provide added value for the more accurate prediction of the treatment efficacy by using a single imaging exam with a blood transcript value [31, 32, 42].

While the uptake per se is considered to be of prognostic significance, measurements of the SUV_{max} are dependent on a number of variables. These, particularly in indolent tumors, often fail to accurately reflect the response to therapy. Although multiple consecutive assessments with visual changes are required, the diverse patient characteristics (SSA treatment, splenic uptake), the PET model (resolution specifics, acquisition mode, acquisition time per bed position, reconstruction method, attenuation correction, and image analysis) as well as image analysis (ROI reconstruction algorithms) can all affect image interpretation [11, 30]. A circulating tumor MAAA can be easily acquired (simple blood draw) at multiple time points in the intervals between sequential receptor PET assessments. Such information can provide added information regarding tumor behavior (proliferative gene expression levels) as well as responses to therapy (decrease in transcript levels) [17].

Monoanalytes, such as CgA, have been used in conjunction with clinical information to aid the interpretation of imaging with varying degrees of clinical efficacy [19, 15]. Many NET patients (~30–50 %) do not have elevated CgA [43], and CgA exhibits low specific metrics with a wide variation in values depending upon the assay type, the laboratory, and numerous coexisting factors (renal insufficiency, proton pump inhibitors) [12]. In our study, CgA was elevated in <60 % of patients, was not correlated with SUV_{max} or Ki-67, and was only related to the secretory component of the circulating gene signature. The genes identified to be most significantly related to CgA levels were *SLC18A2* (VMAT2), well-known as a transporter gene involved in vesicular amine uptake and secretion [44], and *LED1*, involved in transcriptional regulation [45]. As a combinatorial quotient, imaging and CgA, were only poorly correlated with outcome (AUC=0.5, Table 3).

Given the information provided by imaging and Ki-67, inductive logic would suggest that a combinatorial quotient of the two parameters would provide information predictive of outcome. Ki-67 is used as a prognostic clinicopathological surrogate for tumor cell proliferation, forms the basis for the current grading classification, and generally has been used to guide therapeutic strategy [24] despite some reservations (vide European Society for Medical Oncology [46] guidelines). In this study, Ki-67 was not correlated with imaging or the NETest and as a combination with the SUV_{max} was only poorly correlated with outcome. This likely reflects the fact that Ki-67 measures are typically historical (usually measured in the primary early in the course of the disease) and do not provide a real-time evaluation of a dynamic tumor and the well-described evolving proliferative heterogeneity of neoplasia [14]. In the current study, the distribution of Ki-67 was inconsistent between the data sets and could not be extrapolated by generalized linear regression modeling from the circulating gene expression levels. This might reflect the known limitations noted for Ki-67 measurements (different centers; staining protocols, antibodies, and interpreters) but also the

time difference between the blood sampling and the histology. Data set 1 had a median interval of 28 months (range 1–176 months) between the blood collection and the histology, while this was 34 months (range 1–194 months) for data set 2. Another factor that may have influenced the Ki-67 results is the "real-world" situation of patient referral and management, where surgical samples were available for histopathological analysis in 12/27 patients, whereas biopsies were obtained in 7 and cytology in 1, and not repeated in all sites of disease for the majority of subjects. Added value could be provided by real-time dynamic information of tumor status using a circulating signature as a "liquid biopsy." Timed biopsies and blood sampling therefore are required to define whether a circulating measurement could provide a real-time measure of tumor growth.

The successful integration and validation of imaging and biomarker approaches could guide and better define criteria for clinical decisions. In terms of clinical benefit, apart from accurately confirming the presence and status of disease, the most immediate added value would be in the assessment of treatment efficacy. The dimensionality of an MAAA test offers insight into the biological pathways that comprise neoplastic transformation as well as targets for therapy and can provide information for a more accurate assessment of response. A strategy of fusion of not only imaging types (^{68}Ga PET and CT) but imaging and molecular information of disease status is likely to provide added information regarding tumor behavior and response to therapy. Such data promise to be of clinical utility by making available a dynamic measurement which will facilitate a more precise delineation of evolving NET disease in an individual patient.

Compliance with ethical standards

Conflicts of interest None.

Research involving human participants and/or animals Statement of human rights

All procedures performed in studies involving human participants were in accordance with the ethical standards of the institutional and/or national research committee and with the 1964 Declaration of Helsinki and its later amendments or comparable ethical standards.

Statement on the welfare of animals

This article does not contain any studies with animals performed by any of the authors.

Informed consent Informed consent was obtained from all individual participants included in the study.

References

1. Modlin IM, Oberg K, Chung DC, Jensen RT, de Herder WW, Thakker RV, et al. Gastroenteropancreatic neuroendocrine tumours. Lancet Oncol 2008;9(1):61–72. doi:10.1016/s1470-2045(07)70410-2.
2. Hallet J, Law CH, Cukier M, Saskin R, Liu N, Singh S. Exploring the rising incidence of neuroendocrine tumors: a population-based analysis of epidemiology, metastatic presentation, and outcomes. Cancer 2015;121(4):589–97. doi:10.1002/cncr.29099.
3. Kanakis G, Kaltsas G. Biochemical markers for gastroenteropancreatic neuroendocrine tumours (GEP-NETs). Best Pract Res Clin Gastroenterol 2012;26(6):791–802. doi:10.1016/j.bpg.2012.12.006.
4. Kulke MH, Siu LL, Tepper JE, Fisher G, Jaffe D, Haller DG, et al. Future directions in the treatment of neuroendocrine tumors: consensus report of the National Cancer Institute Neuroendocrine Tumor clinical trials planning meeting. J Clin Oncol Off 2011;29(7):934–43. doi:10.1200/jco.2010.33.2056.
5. Modlin IM, Moss SF, Chung DC, Jensen RT, Snyderwine E. Priorities for improving the management of gastroenteropancreatic neuroendocrine tumors. J Natl Cancer Inst 2008;100(18):1282–9. doi:10.1093/jnci/djn275.
6. de Mestier L, Dromain C, d'Assignies G, Scoazec JY, Lassau N, Lebtahi R, et al. Evaluating neuroendocrine tumors progression and therapeutic response: state of the art. Endocr Relat Cancer 2013;18:18.
7. Sundin A, Rockall A. Therapeutic monitoring of gastroenteropancreatic neuroendocrine tumors: the challenges ahead. Neuroendocrinology 2012;96(4):261–71. doi:10.1159/000342270.
8. Castaño JP, Sundin A, Maecke HR, Villabona C, Vazquez-Albertino R, Navarro E, et al. Gastrointestinal neuroendocrine tumors (NETs): new diagnostic and therapeutic challenges. Cancer Metastasis Rev 2014;33:353–9. doi:10.1007/s10555-013-9465-1.
9. Faivre S, Ronot M, Dreyer C, Serrate C, Hentic O, Bouattour M, et al. Imaging response in neuroendocrine tumors treated with targeted therapies: the experience of sunitinib. Target Oncol 2012;7(2):127–33. doi:10.1007/s11523-012-0216-y.
10. Toumpanakis C, Kim MK, Rinke A, Bergestuen DS, Thirlwell C, Khan MS, et al. Combination of cross-sectional and molecular imaging studies in the localization of gastroenteropancreatic neuroendocrine tumors. Neuroendocrinology 2014;99:63–74.
11. Bodei L, Kidd M, Prasad V, Baum RP, Drozdov I, Modlin IM. The future of nuclear medicine imaging of neuroendocrine tumors: on a clear day one might see forever. Eur J Nucl Med Mol Imaging 2014;41:2189–93. doi:10.1007/s00259-014-2836-1.
12. Modlin I, Drozdov I, Alaimo D, Callahan S, Teixeira N, Bodei L, et al. A multianalyte PCR blood test outperforms single analyte ELISAs (chromogranin A, pancreastatin, neurokinin A) for neuroendocrine tumor detection. Endocr Relat Cancer 2014;21:615–28.
13. Rindi G, Petrone G, Inzani F. The 2010 WHO classification of digestive neuroendocrine neoplasms: a critical appraisal four years after its introduction. Endocr Pathol 2014;25(2):186–92. doi:10.1007/s12022-014-9313-z.
14. Yang Z, Tang LH, Klimstra DS. Gastroenteropancreatic neuroendocrine neoplasms: historical context and current issues. Semin Diagn Pathol 2013;30(3):186–96. doi:10.1053/j.semdp.2013.06.005.
15. Modlin IM, Gustafsson BI, Pavel M, Svejda B, Lawrence B, Kidd M. A nomogram to assess small-intestinal neuroendocrine tumor ('carcinoid') survival. Neuroendocrinology 2010;92(3):143–57. doi:10.1159/000319784.
16. Modlin IM, Drozdov I, Kidd M. The identification of gut neuroendocrine tumor disease by multiple synchronous transcript analysis in blood. PLoS One 2013;8(5):e63364. doi:10.1371/journal.pone.0063364.
17. Modlin I, Drozdov I, Kidd M. A multitranscript blood neuroendocrine tumor molecular signature to identify treatment efficacy and disease progress. J Clin Oncol 2013;31(Suppl):abstract 4137.
18. Modlin I, Drozdov I, Kidd M. Gut neuroendocrine tumor blood qPCR fingerprint assay: characteristics and reproducibility. Clin Chem Lab Med 2014;52(3):419–29.

19. Giandomenico V, Modlin IM, Ponten F, Nilsson M, Landegren U, Bergqvist J, et al. Improving the diagnosis and management of neuroendocrine tumors: utilizing new advances in biomarker and molecular imaging science. Neuroendocrinology 2013;98(1):16–30. doi:10.1159/000348832.
20. Oken MM, Creech RH, Tormey DC, Horton J, Davis TE, McFadden ET, et al. Toxicity and response criteria of the Eastern Cooperative Oncology Group. Am J Clin Oncol 1982;5(6):649–55.
21. Eisenhauer EA, Therasse P, Bogaerts J, Schwartz LH, Sargent D, Ford R, et al. New response evaluation criteria in solid tumours: revised RECIST guideline (version 1.1). Eur J Cancer 2009;45(2):228–47. doi:10.1016/j.ejca.2008.10.026.
22. Virgolini I, Ambrosini V, Bomanji JB, Baum RP, Fanti S, Gabriel M, et al. Procedure guidelines for PET/CT tumour imaging with 68Ga-DOTA-conjugated peptides: 68Ga-DOTA-TOC, 68Ga-DOTA-NOC, 68Ga-DOTA-TATE. Eur J Nucl Med Mol Imaging 2010;37(10):2004–10. doi:10.1007/s00259-010-1512-3.
23. Baum RP, Kulkarni HR. THERANOSTICS: from molecular imaging using Ga-68 labeled tracers and PET/CT to personalized radionuclide therapy - the Bad Berka experience. Theranostics 2012;2(5):437–47. doi:10.7150/thno.3645.
24. Rindi G, Klimstra DS, Arnold R, Kloppel G, Bosman FT, Komminoth P, et al. Nomenclature and classification of neuroendocrine neoplasms of the digestive system. In: Bosman FT, Carneiro F, Hruban RH, Theise ND, editors. WHO classification of the digestive system. 4th ed. Lyon: International Agency for Research on Cancer; 2010.
25. Travis WD, Brambilla E, Muller-Hermelink HK, Harris CC. Pathology and genetics of tumours of the lung, pleura, thymus and heart. 2004.
26. Friedman J, Hastie T, Tibshirani R. Regularization paths for generalized linear models via coordinate descent. J Stat Softw 2010;33(1):1–22.
27. Kuhn M. Building predictive models in R using the caret package. J Stat Softw 2008;28(5):1–26.
28. Hanley JA, McNeil BJ. The meaning and use of the area under a receiver operating characteristic (ROC) curve. Radiology 1982;143(1):29–36.
29. Treglia G, Castaldi P, Rindi G, Giordano A, Rufini V. Diagnostic performance of gallium-68 somatostatin receptor PET and PET/CT in patients with thoracic and gastroenteropancreatic neuroendocrine tumours: a meta-analysis. Endocrine 2012;42(1):80–7. doi:10.1007/s12020-012-9631-1.
30. Ruf J, Schiefer J, Kropf S, Furth C, Ulrich G, Kosiek O, et al. Quantification in Ga-DOTA(0)-Phe(1)-Tyr(3)-octreotide positron emission tomography/computed tomography: can we be impartial about partial volume effects? Neuroendocrinology 2013;97(4):369–74. doi:10.1159/000350418.
31. Campana D, Ambrosini V, Pezzilli R, Fanti S, Labate AM, Santini D, et al. Standardized uptake values of (68)Ga-DOTANOC PET: a promising prognostic tool in neuroendocrine tumors. J Nucl Med 2010;51(3):353–9. doi:10.2967/jnumed.109.066662.
32. Haug AR, Auernhammer CJ, Wängler B, Schmidt GP, Uebleis C, Göke B, et al. 68Ga-DOTATATE PET/CT for the early prediction of response to somatostatin receptor-mediated radionuclide therapy in patients with well-differentiated neuroendocrine tumors. J Nucl Med 2010;51(9):1349–56. doi:10.2967/jnumed.110.075002.
33. Sharma P, Naswa N, Kc SS, Alvarado LA, Dwivedi AK, Yadav Y, et al. Comparison of the prognostic values of 68Ga-DOTANOC PET/CT and 18F-FDG PET/CT in patients with well-differentiated neuroendocrine tumor. Eur J Nucl Med Mol Imaging 2014;41:2194–202.
34. Kwekkeboom DJ, Kam BL, van Essen M, Teunissen JJ, van Eijck CH, Valkema R, et al. Somatostatin-receptor-based imaging and therapy of gastroenteropancreatic neuroendocrine tumors. Endoc Relat Cancer 2010;17(1):R53–73. doi:10.1677/erc-09-0078.
35. Walenkamp A, Crespo G, Fierro Maya F, Fossmark R, Igaz P, Rinke A, et al. Hallmarks of gastrointestinal neuroendocrine tumours: implications for treatment. Endocr Relat Cancer 2014;21(6):R445–60. doi:10.1530/erc-14-0106.
36. Kaemmerer D, Peter L, Lupp A, Schulz S, Sänger J, Prasad V, et al. Molecular imaging with (68)Ga-SSTR PET/CT and correlation to immunohistochemistry of somatostatin receptors in neuroendocrine tumours. Eur J Nucl Med Mol Imaging 2011;38(9):1659–68. doi:10.1007/s00259-011-1846-5.
37. Corleto VD, Nasoni S, Panzuto F, Cassetta S, Delle Fave G. Somatostatin receptor subtypes: basic pharmacology and tissue distribution. Dig Liver Dis 2004;36 Suppl 1:S8–16.
38. Velikyan I, Sundin A, Sörensen J, Lubberink M, Sandström M, Garske-Román U, et al. Quantitative and qualitative intrapatient comparison of 68Ga-DOTATOC and 68Ga-DOTATATE: net uptake rate for accurate quantification. J Nucl Med 2014;55(2):204–10. doi:10.2967/jnumed.113.126177.
39. Scheibe M, Arnoult N, Kappei D, Buchholz F, Decottignies A, Butter F, et al. Quantitative interaction screen of telomeric repeat-containing RNA reveals novel TERRA regulators. Genome Res 2013;23(12):2149–57. doi:10.1101/gr.151878.112. **Epub 2013 Aug 6**.
40. Marinoni I, Kurrer AS, Vassella E, Dettmer M, Rudolph T, Banz V, et al. Loss of DAXX and ATRX are associated with chromosome instability and reduced survival of patients with pancreatic neuroendocrine tumors. Gastroenterology 2014;146(2):453–60. doi:10.1053/j.gastro.2013.10.020.
41. Kayani I, Bomanji JB, Groves A, Conway G, Gacinovic S, Win T, et al. Functional imaging of neuroendocrine tumors with combined PET/CT using 68Ga-DOTATATE (DOTA-DPhe1, Tyr3-octreotate) and 18F-FDG. Cancer 2008;112(11):2447–55. doi:10.1002/cncr.23469.
42. Ezziddin S, Lohmar J, Yong-Hing CJ, Sabet A, Ahmadzadehfar H, Kukuk G, et al. Does the pretherapeutic tumor SUV in 68Ga DOTATOC PET predict the absorbed dose of 177Lu octreotate? Clin Nucl Med 2012;37(6):e141–7. doi:10.1097/RLU.0b013e31823926e5.
43. Lindholm DP, Oberg K. Biomarkers and molecular imaging in gastroenteropancreatic neuroendocrine tumors. Horm Metab Res 2011;43(12):832–7. doi:10.1055/s-0031-1287794.
44. Jakobsen AM, Andersson P, Saglik G, Andersson E, Kölby L, Erickson JD, et al. Differential expression of vesicular monoamine transporter (VMAT) 1 and 2 in gastrointestinal endocrine tumours. J Pathol 2001;195(4):463–72.
45. Rozenblatt-Rosen O, Hughes CM, Nannepaga SJ, Shanmugam KS, Copeland TD, Guszczynski T, et al. The parafibromin tumor suppressor protein is part of a human Paf1 complex. Mol Cell Biol 2005;25(2):612–20.
46. Öberg K, Knigge U, Kwekkeboom D, Perren A. Neuroendocrine gastro-entero-pancreatic tumors: ESMO Clinical Practice Guidelines for diagnosis, treatment and follow-up. Ann Oncol 2012;23(Suppl 7):vii124–30.